doi:10.1016/j.jmb.2006.11.037 J. Mol. Biol. (2007) 366, 216–229

JMB

Available online at www.sciencedirect.com

ScienceDirect

ELSEVIER

The Crystal Structures of Human Calpains 1 and 9 Imply Diverse Mechanisms of Action and Auto-inhibition

Tara L. Davis, John R. Walker, Patrick J. Finerty Jr, Farrell Mackenzie Elena M. Newman and Sirano Dhe-Paganon*

Structural Genomics Consortium and the Department of Physiology University of Toronto 100 College St, Toronto, ON Canada M5G 1L5

*Corresponding author

Calpains are calcium activated cysteine proteases found throughout the animal, plant, and fungi kingdoms; 14 isoforms have been described in the human genome. Calpains have been implicated in multiple models of human disease; for instance, calpain 1 is activated in the brains of individuals with Alzheimer's disease, and the digestive tract specific calpain 9 is down-regulated in gastric cancer cell lines. We have solved the structures of human calpain 1 and calpain 9 protease cores using crystallographic methods; both structures have clear implications for the function of non-catalytic domains of full-length calpains in the calcium-mediated activation of the enzyme. The structure of minicalpain 1 is similar to previously solved structures of the protease core. Auto-inhibition in this system is most likely through rearrangements of a central helical/loop region near the active site cysteine, which occlude the substrate binding site. However, the structure of minicalpain 9 indicates that auto-inhibition in this enzyme is mediated through large intra-domain movements that misalign the catalytic triad. This disruption is reminiscent of the full-length inactive calpain conformation. The structures of the highly conserved, ubiquitously expressed human calpain 1 and the more tissue specific human calpain 9 indicate that although there are high levels of sequence conservation throughout the calpain family, isolated structures of family members are insufficient to explain the molecular mechanism of activation for this group of proteins.

Keywords: cysteine protease; structure; peptidase; active site; autoinhibition

Introduction

Calpains (EC 3.4.22.17) are calcium activated cysteine proteases containing a catalytic domain most closely related to that of papain. Calpains are found throughout the animal, plant, and fungi kingdoms; 14 isoforms have been described in the human genome to date.[1–3] There are two classes of calpains; those expressed ubiquitously and those which are expressed in a tissue-specific fashion. Of the ubiquitous calpains, the μ-calpain (calpain 1) and m-calpain (calpain 2) isoforms have been extensively studied with respect to structure and function *in vitro* and *in vivo*.[2] These "classical" calpains exist in cells as heterodimers of a large subunit comprised of four domains associated with a small subunit. Activation of calpain is a calcium dependent process and involves multiple structural changes followed by limited autoproteolysis to form active calpain enzyme.[2,4–6] Extended activation of calpains leads to further autoproteolysis, finally leading to stable protease-resistant cores of 50, 40, and 26 kDa for proteolysis of calpain 2 by calpain 1.[2,4,5] Calpains are not proenzymes, however; the unproteolyzed heterodimer of calpain 1 and calpain 2 is enzymatically active in the presence of calcium, although in the cell and under physiological conditions it is thought that activation will be concomitant with autoproteolysis.[5,7]

The expression levels and activity states of both ubiquitous and tissue-specific calpains have been implicated in several models of human disease. Calpain 1 is activated in the brains of individuals with Alzheimer's disease[8,9] and the proteolytic cleavage of beta-amyloid precursor protein and tau protein by calpain 1 might be involved in plaque formation.[8,10–12] In the eye, calpain 2 and a lens-specific variant of calpain 3 are responsible for

Abbreviations used: β-ME, β-mercaptoethanol; sLY-AMC, succinyl-Leu-Tyr-(7-amino-4-methylcoumarin).

E-mail address of the corresponding author: sirano.dhepaganon@utoronto.ca

proteolytic cleavages of α and β-crystallin which when overactivated can lead to cataract formation.[1,8,13,14] Over 100 independent mutants of the muscle-specific isoforms of calpain 3 have been reported to be pathologically associated with limb girdle muscular dystrophy type 2A,[15–17] and positional cloning has identified calpain 10 gene variants associated with type 2 diabetes.[18–21] Interestingly, the digestive-tract-specific calpain 9 is down-regulated in gastric cancer cell lines, and depletion of calpain 9 using antisense RNA resulted in transformation and tumorigenesis in fibroblasts, suggesting calpain 9 is acting as a tumor suppressor in those systems.[22,23] In addition, down-regulation of calpain 9 has recently been linked to hypertensive heart and kidney disease in salt-sensitive Dahl rats.[24] Therefore, understanding the molecular mechanisms of both activation and inactivation of calpains are research topics of interest, since both states of the calpain enzyme are implicated in disease.

The domain architecture of both calpain 1 and 9 consists of a short N-terminal extension (domain I or dI), the catalytic core (dII), the C2-like domain dIII, and a penta-EF hand domain dIV, which interacts with the small subunit domains dV and dVI. A construct containing the isolated catalytic domains IIa and IIb of calpain has been termed the "minicalpain". The minicalpains of rat calpain 1 and rat calpain 2 have previously been characterized both enzymatically and structurally.[25–28] The minicalpain of rat calpain 1 shows similar enzymatic characteristics compared to the intact enzyme[26] and the crystal structure of an inactive mutant of rat minicalpain 1 shows that the domains IIa and IIb are conformationally competent to perform catalysis.[25] Rat minicalpain 2, in contrast, was found to be 10,000 times less active than the full-length calpain 2 protein. Based on the crystal structure of rat minicalpain 2, this loss of activity was attributed to auto-inhibition of the minicalpain construct *via* dynamic instability of the α7 helix and blockage of the active site by a conserved tryptophan residue found next to the active site cysteine.[26] Structural genomic studies of the human minicalpains are expected to yield a wealth of information about the active sites of these biologically relevant molecules, including structural analysis of the substrate binding surface and the regions surrounding the catalytic triad. Presented here are the X-ray crystallographic structures of two human minicalpains: calpain 1 and calpain 9. Although the study of these structures to aid in drug design is ongoing and expected to be fruitful, it is also clear that both of these structures raise questions about the fundamental molecular mechanism of minicalpain auto-inactivation.

Results

The overall architecture of human minicalpain 1, comprising the catalytic IIa and IIb domains of the enzyme (residues 29–360), retains the classical mixed α/β structure typical of these papain-like proteins,[2,29–31] (Figure 1). There are two molecules of human minicalpain 1 in the asymmetric unit; included in the models are three sites of modification by β-mercaptoethanol (β-ME), including the active site cysteine in one of the two molecules. The other β-ME modification is identical in both molecules of the asymmetric unit and is on Cys351, removed from the active site. The two protein chains are superimposable with an RMSD value of 0.4 Å. In general, *B* factors throughout the core of the molecule are well-behaved, with an average *B* factor of 44 $Å^2$ for main-chain and side-chain atoms; two exceptions are the region around residues 206–224 and the region including residues 253–267, which have average *B* factors around 80 $Å^2$. These regions correspond to the dynamic α7 region, which is helical in some minicalpain structures and a loop in others (including the structure of human minicalpain 1), and the second gating loop found C-terminal to the α7 region. No density is observed for the N-terminal 23 residues of the construct, including the $(His)_6$ tag and residues 29–32 of calpain 1, or for the C-terminal six residues of the construct (Pro355–Ser360).

The crystal structure of the protease core of human calpain 1, solved in absence of substrate or inhibitor, is quite similar to the structures of rat minicalpain 1 and rat minicalpain 2 described previously.[25,26] Human minicalpain 1 aligns with an RMSD value of 0.9 Å to rat minicalpain 1 (PDB ID 1KXR; alignment performed over 322 Cα atoms), and with an RMSD value of 0.6 Å to rat minicalpain 2 (PDB ID 1MDW, 321 Cα atoms used for the alignment).[25,26] This is not completely surprising; the sequence identity across the amino acids in the crystal structures is 87% for human and rat minicalpain 1, and 71% for human minicalpain 1 and rat minicalpain 2. The catalytic triads of all three structures are in identical conformations (Figures 1(b) and 2). The network of acidic amino acids and ordered water molecules which form coordination sites for calcium ions in both the IIa and IIb subdomains are intact, as is the Arg104–Glu333 salt bridge that connects the two calcium binding sites (Figure 1(c)). However, there were two regions in the human minicalpain 1 structure which were clearly in novel conformations: a conserved Trp116 residue in the α4 helix just C-terminal to the catalytic cysteine residue and the residues from Ser206–Gly220 which make up the α6–α7 loop and the α7 region (Figure 2).

Rat minicalpain 1 was the first minicalpain construct to be analyzed structurally; the main mechanism of auto-inhibition was found to be the calcium binding sites in sub-domains IIa and IIb, and indeed in the presence of calcium rat minicalpain 1 is much more active than the other minicalpains subsequently studied, although still several orders of magnitude less active than full-length enzyme.[25,26] The rat minicalpain 2 structure, by comparison with rat minicalpain 1, identified two sites of auto-inhibition in addition to the calcium

binding sites; the α7 region, which is helical in rat minicalpain 1 and a disordered loop in rat minicalpain 2, and the region of α4 containing the catalytic cysteine and a neighboring tryptophan residue (Figure 2).[25,26] Trp116, following the numbering of human minicalpain 1, is one of the most conserved residues in the calpain catalytic domain; the only two cases of substitution among the 14 human isoforms are in the non-catalytic calpain 6 and the highly divergent family member calpain 7. In the rat minicalpain 2 structure the analogous Trp106 residue is protruding into the active site of the catalytic domain, accompanied by movements in the α7 region, including the insertion of Phe204 into the void left behind by the movement of Trp106. In addition, the N terminus of α7 and the loop preceding it become disordered in the minicalpain 2 structure (Figure 2). This coordinated hydrophobic core collapse and rearrangement of the α7 region provides an elegant picture of the potential mechanism of auto-inhibition in rat minicalpain 2. However, Trp116 is not in the proper conformation in our structure to perform this function (Figures 3 and 4). Instead, the indole amine of the Trp116 side-chain is stabilized by interactions with the side-chain oxygen atoms of Ser211 (3.44 Å) and Glu349 (3.20 Å to $O^{\delta 1}$), as well of the oxygen of a β-ME molecule attached to Cys351 (3.2 Å) (Figure 3). Instead of playing a role in stabilizing the hydrophobic core interactions between sub-domains IIa and IIb, Phe214 is now shifted closer to the active site cysteine, perhaps stabilized by the interaction between Ser211 and Trp116 (Figures 2 and 3). This shift of the α7 region now allows the region disordered in the minicalpain 2 structure to lie across the substrate binding site (Figure 2). Indeed, the similarity between the orientation of the Cα trace of residues Gly208–Glu212 and the orientation of the tight-binding inhibitor leupeptin found in the rat minicalpain 1 structure is striking[27] (Figure 2). In addition to aromatic and aliphatic interactions, stabilization of this orientation of the α7 loop is through the interaction between Ser211 and Gln349, Thr210 and Arg347, and Ser209 and Asp253 *via* water molecules (Figure 3). Unfortunately, the Trp106Ala mutant of rat minicalpain 2 does not remove auto-inhibition of the enzyme, perhaps due to misfolding of the enzyme,[26] so the importance of this residue in an auto-inhibited mechanism cannot be tested enzymatically. However, based on the crystal structures of rat minicalpain 1, rat minicalpain 2, and human minicalpain 1, the coupled movements of the α7 region and the tryptophan residue in α4 seem to play the largest role in auto-inhibition for these isoforms, and the dynamic nature of these interactions are reflected by the different conformations in which they are trapped in various crystal structures.

The crystal structure of human minicalpain 9 (residues 28–347 in the construct) contains one molecule in the asymmetric unit and is modified by β-ME at the active site Cys97 and the distal Cys334, analogous to the minicalpain 1 structure (Figure 4). No density is seen for the N-terminal $(His)_6$ tag or linker region contributed by the vector, or for the C-terminal ten residues in the construct (Pro338–His347). *B* factors throughout the 309 amino acids visible in the structure are well behaved (average: 45 $Å^2$ for main-chain and side-chain atoms), with the exception of a group of residues from Pro49–Val66 with higher *B* factors (average 76 $Å^2$). Two residues (Glu59 and Arg60) in this region are disordered and residues 61–63 have *B* factors above 100 $Å^2$. This region is the N-terminal gating loop; it is interesting to note that one of the gating loops in the minicalpain 1 (the C-terminal loop) is also a site of elevated *B* factors. Perhaps this is indicative of dynamic conformational sampling of these regions in the protein when the active site is unoccupied.

The crystal structure of human minicalpain 9 has significant structural dissimilarity to other minicalpain structures (Figure 4); an attempt to align minicalpain 9 with minicalpain 1 yields an RMSD value of 7 Å across 309 Cα atoms. However, the individual sub-domains of minicalpain 9 align nicely with minicalpain 1; sub-domain IIa (residues Phe29 – Lys188) aligns with an RMSD value of 0.7 Å to the corresponding residues in minicalpain 1, while sub-domain IIb (Gly201–Thr337) aligns with an RMSD value of 0.6 Å. The α7 region has been omitted from this analysis; minicalpain 9 forms an α-helix in this region whilst minicalpain 1, which has a glycine at position 213, forms a loop (compare Figure 1 to Figure 4). Upon closer analysis, it is not the fold itself which has changed, but rather the relationship between sub-domains IIa and IIb. The catalytic triad is disrupted in minicalpain 9; the distance between the catalytic cysteine and the $N\delta^1$ atom of His254 is 12 Å as compared to the 3.9 Å distance between the equivalent atoms in the calpain 1 active site (Figure 4). Minicalpain 9 contains the two conserved Ca^{2+} binding sites found in other minicalpain structures, but although two Ca^{2+} ions are clearly seen in these sites the two residues involved in the salt bridge between the two sub-domains (Arg86 and Glu316) are ~17 Å away from each other. The effect of these differences taken on a

Figure 1. (a) Structure of human minicalpain 1. The fold of human minicalpain 1 is shown in ribbon representation. The structure is colored by secondary structure elements, and the N and C termini are labeled. The catalytic triad is shown in stick representation and labeled, and the two calcium ions bound in the crystal structure are shown as yellow spheres. The numbering is, when possible, as by Moldoveanu *et al.*[25] (b) The active site of human minicalpain 1 shown in stick representation and labeled, as are selected secondary elements. (c) Key residues from the protein which coordinate calcium are shown in stick representation and labeled; several ordered water molecules also participate in calcium coordination, but for the sake of clarity are not shown here. Also depicted is the salt bridge between Arg104 and Glu333, which links the two binding sites.

global level is that sub-domain IIb is rotated 45° and about 12 Å away from sub-domain IIa (Figure 4). This is likely to represent an auto-inhibited conformation for minicalpain 9, as the catalytic triad is not competent for catalysis in this structure and the salt bridge linking the two sub-domains together

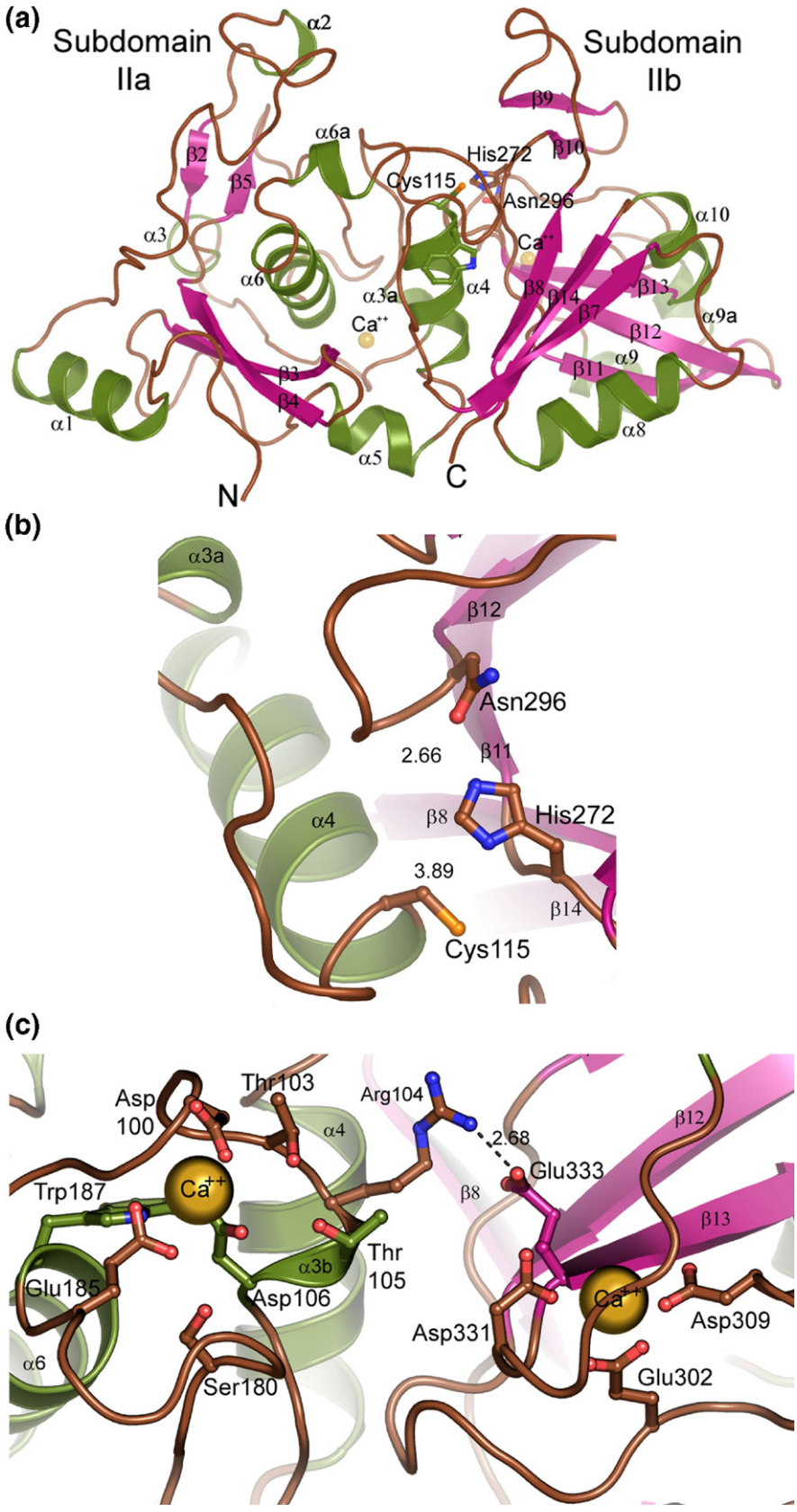

Figure 1 (*legend on previous page*)

cannot be formed. Indeed, the structure of minicalpain 9 is in many ways similar to the full-length structures of inactive, calcium-free calpains which represent the basal state of the enzyme[32,33] (Figure 5). The low but clearly measurable activity observed towards the succinyl-Leu-Tyr-(7-amino-4-methyl-coumarin) (sLY-AMC) and BODIPY-casein substrates (Table 1 and Figure 5) further show that minicalpain 9 is not misfolded and that the structure represents an auto-inhibited state that is predominantly sampled in solution. It is interesting to note that even in the context of a pre-formed α7 helix

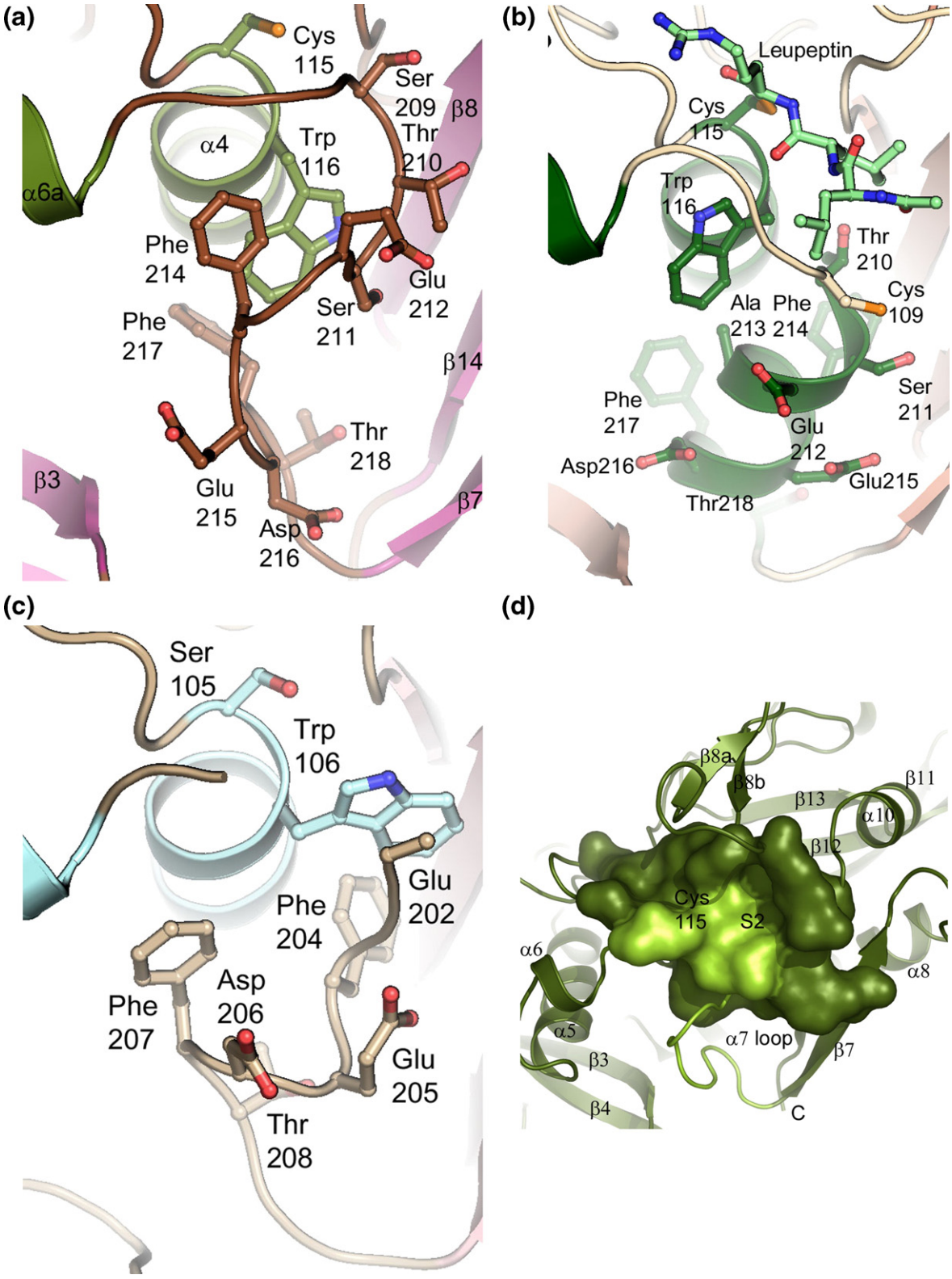

Figure 2 (*legend on next page*)

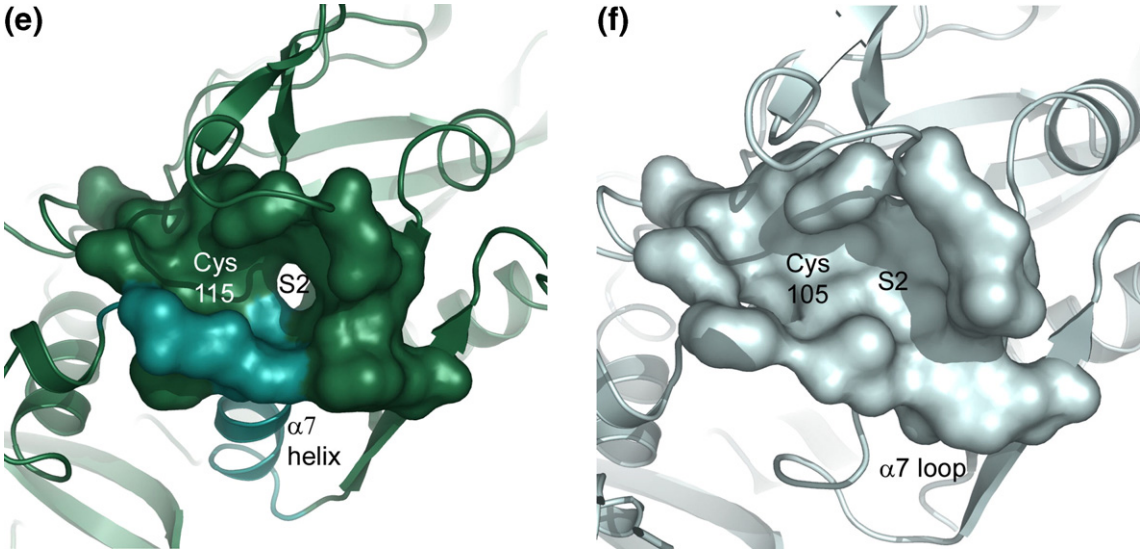

Figure 2. Comparison of the α7 region in minicalpain structures. (a) The α7 region of human minicalpain 1. The protein is shown in ribbon representation, with α7 residues (Ser209–Asp216) shown in stick representation for emphasis, as is Trp116. The relative position of catalytic Cys115 is shown as a reference. (b) The α7 region of rat minicalpain 1. This structure was solved in the presence of the covalent inhibitor leupeptin, shown in stick representation in light green. The presence of an alanine instead of a glycine at position 213 leads to the formation of the α7 helix in the minicalpain structure, as compared to the region shown in (a). (c) The α7 region of rat minicalpain 2. The catalytic cysteine has been mutated into a serine, shown in position 105. The tryptophan residue at position 106 was previously proposed as a key player in the mechanism of auto-inactivation of this minicalpain.[26] Residues 198–201 which comprise the N-terminal region of α7 are disordered in this structure. (d) The substrate binding surface of human minicalpain 1 is shown in olive green. All structures are shown in ribbon representation, with the residues comprising the catalytic site and substrate binding surface shown as surfaces. The catalytic cysteine and S2 surface are labeled; the α7 helix is labeled, colored in light green and shown in both cartoon and surface representation. (e) The substrate binding surface of rat minicalpain 1 is shown in dark teal. Secondary structural elements are labeled, as are the region of the surface contributed by the active site cysteine and the location of the S2 surface. The α7 region is shaded a lighter teal for emphasis. (f) The substrate binding surface of rat minicalpain 2 is shown in light blue. Secondary structural elements and key residues are labeled as in (d) and (e). Relatively small changes in the region around the active site cysteine and the α7 region induce quite large structural changes in the surface presented by the minicalpain to substrate.

(due to an alanine at position 195 instead of the helix-breaking glycine substitution found in calpain 1) (Figure 4), minicalpain 9 is auto-inhibited in solution to the same extent as human minicalpain 1. One might have expected human minicalpain 9 to have activity more similar to that of rat minicalpain 1, whose high catalytic efficiency against the sLY-AMC substrate has previously been ascribed to the presence of such a pre-formed helix (Table 1).[25,26] Based on the conformation of minicalpain 9 captured in the crystal structure, it is clear that alternate mechanisms of auto-inhibition must exist for at least this calpain isoform.

The molecular functions of calpain 9 and identity of its substrates are unknown. Therefore, the current structure of calpain 9 and the analysis of the putative substrate binding surfaces may afford insight into substrate specificity and provide clues to its natural substrates. Like most proteases, sub-sites adjacent to the catalytic cysteine of calpains form the basis of functional specificity. For calpains 1 and 2, the S1 and S2 sub-sites appear to be most important determinants for substrate specificity.[27,34,35] Structural studies of the leupeptin and E64 inhibited enzymes show that the S1 site is formed by two gating loops, one from each lobe, which clamp down on the P1 side-chain.[27] The S2 site is a sink for hydrophobic P2 residues.[27] These sites are identical in calpain 1 and calpain 2, but the corresponding sub-sites of calpain 9 are lined with residues that are different and likely provide altered specificity for substrate binding.[27] Notably, the S1 clamp of calpain 9 is formed by a significantly shortened N-terminal gating loop (residues Ser58–Pro61, α1–β1a loop). This region of calpain 9 also shows a high degree of disorder perhaps suggesting that calpain 9 does not form a well-defined S1 sub-site in the absence of substrate. This may even suggest that calpain 9 does not require significant specificity at this peptide position for function. On the other hand, the epsilon amino group of Lys188 in the α6–α7 loop is poised to interact with a side-chain of the P1 residue of substrate. This is a function that in calpain 1 is performed by an acidic gating loop 1 residue (Glu72 in the α2–β2 loop), and again suggests an altered specificity for substrate at this position. The P2 sub-site of calpain 9 is also different compared with calpains 1 or 2; a serine to phenylalanine substitution (Phe233) at the base of the P2 sub-site in calpain 9 suggests a preference for smaller, aliphatic residues. These small amino acid differences between calpain 1 and calpain 9 may allow for the specific design of

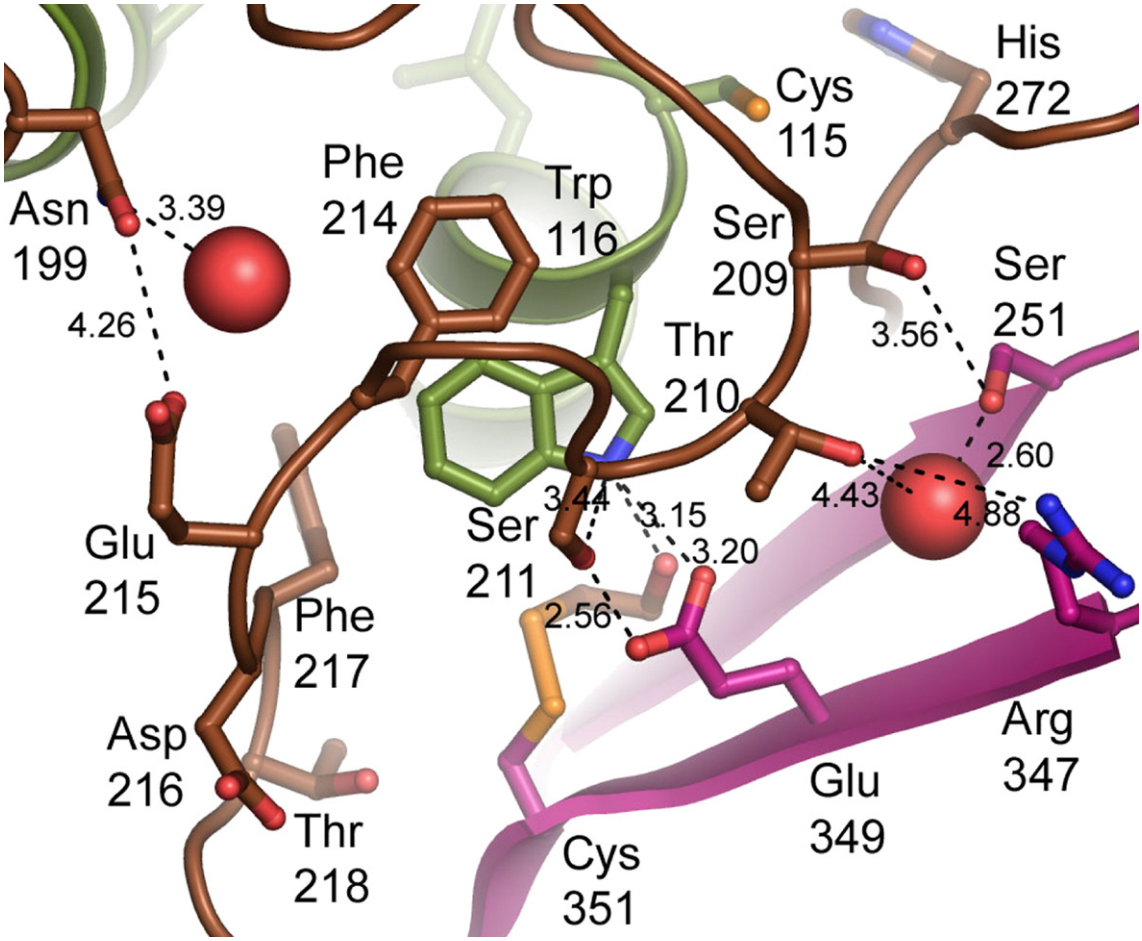

Figure 3. The structural environment around Trp116 and the spatial relationship between α7 and α4 in human minicalpain 1. The β-ME molecule modifying the distal Cys351 residue is shown in stick representation; distances between either electrostatic pairs or water molecules are given in Angstrom units.

therapeutic inhibitors as well as diagnostic reagents against the tissue-specific calpain 9.

Discussion

The current model of calpain activation includes calcium dependent release of the catalytic domain from a repressed conformation. In the full-length enzyme, non-catalytic supporting domains dI, dIII, dIV, and dVI provide a foundation such that the two lobes of the papain-like catalytic domain are kept apart until calcium binding triggers activation.[33,36,37] In the absence of calcium, the carboxy-terminal end of the catalytic domain is covalently fixed to one corner of the foundation (leading into the C2-like domain III) and the amino-terminal peptide (domain I) is non-covalently fixed to the opposing corner. Calcium binding to dIV and dVI releases their grip on the amino-terminal peptide, freeing the catalytic lobes for assembly and catalytic competency. The latter process also requires binding of two calcium atoms in each of the catalytic lobes, leading to the stabilization of a salt bridge and orientation of the two lobes.[25,32,33,36] As an added level of complexity, the non-catalytic domains may also provide auxiliary interactions needed for full catalytic activity. Notably, dIII interacts and stabilizes the helical form of region α7 of calpain 2, which abuts the active site.[32,33,36,37] In the absence of this interaction, α7 (as in the structure of the minicalpain 2 construct) can adopt a random coil conformation that subsequently allows rotation of the aromatic side-chain of a neighboring conserved tryptophan (Trp116) into the S2 sub-site, interfering with binding of calpain substrates. The conformational flexibility in α7 has been attributed to a centrally located glycine residue found in about half of calpain isoforms, including rat calpain 2 and human calpain 1.[26] The rat homolog of calpain 1 has an alanine at that position in α7, adopts the helical conformation even in absence of regulatory domains, and is more active in solution, thereby validating the requirement of a helical α7 for catalysis for calpains.[25,26] Stabilization of the α7 region in order to obtain a catalytically competent enzyme is clearly necessary for human calpain 1 as well, based on our crystal structure. As in the case of rat minicalpain 2, human minicalpain 1 encodes an α7 region which is found in a random coil conformation. Presumably at least one of the functions of the non-catalytic domains for human calpain 1 is to stabilize the α7 region into a productive conformation for catalysis.

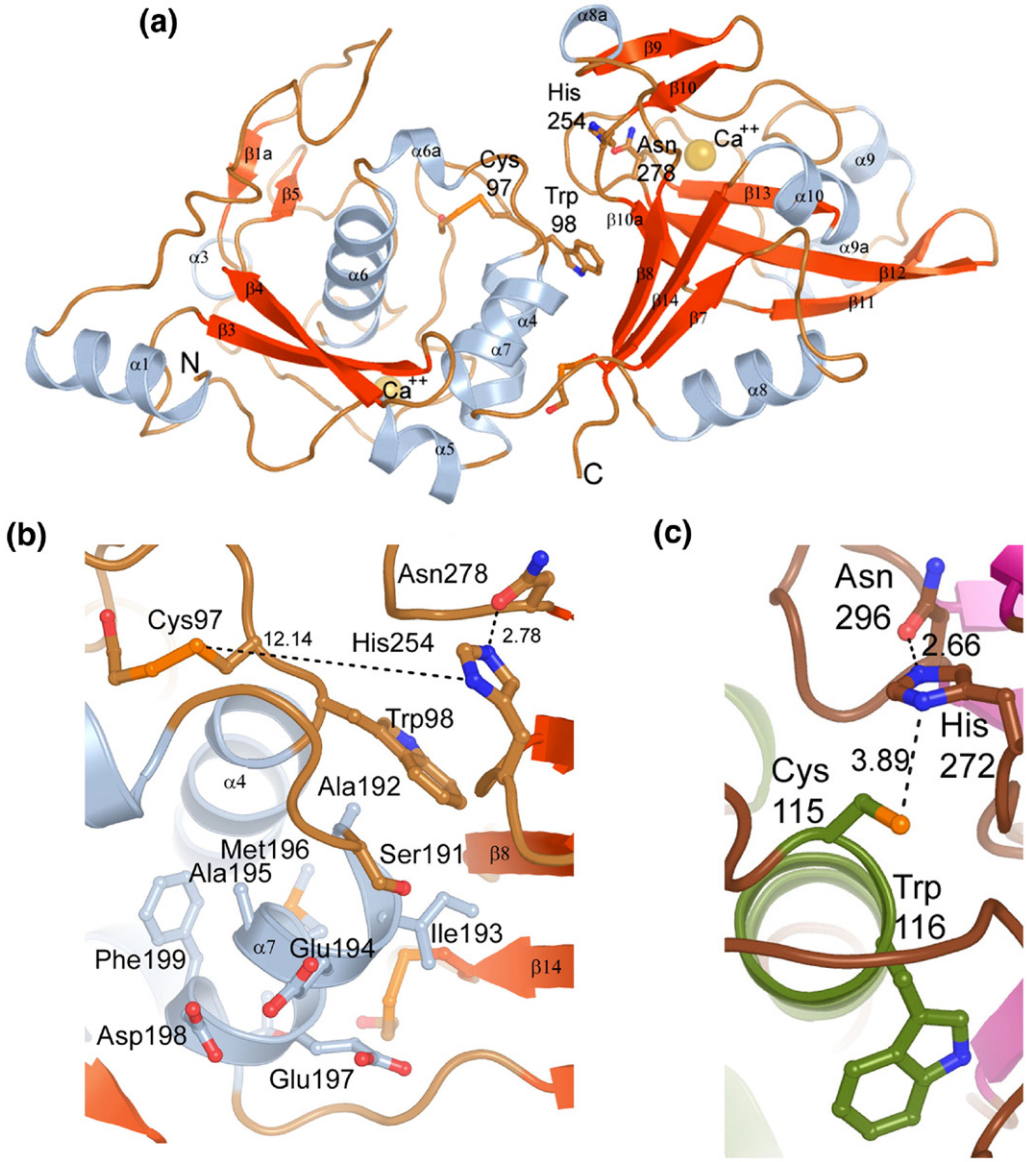

Figure 4. The structure of human minicalpain 9. (a) The fold of human minicalpain 9 is shown in ribbon representation. The structure is colored by secondary structure elements, and the N and C termini are labeled. The catalytic triad is shown in stick representation and labeled, and the two calcium ions bound in the crystal structure are shown as yellow spheres. (b) Zoomed view of the malformed active site in human minicalpain 9. The alanine in position 195 stabilizes the formation of the α7 helix; other residues conserved between human minicalpains 1 and 2 are divergent in this family member. The distance between the catalytic and the histidine and asparagine of the catalytic triad are shown. (c) The active site of human minicalpain 1 for comparison to (b).

Since non-catalytic domains are necessary for full catalytic activity of calpains, auto-inhibition has been hypothesized to occur if proteolytic degradation causes release of the catalytic core domains IIa and IIb. This would add yet another layer of regulation to the calpain system, preventing the potentially catastrophic effects of a runaway protease inside the cell. Our structure of human calpain 1 shows that auto-inhibition occurs not through steric obstruction of the S2 sub-site by Trp116, but instead through blockade of the S2 sub-site by several residues from the α7 region. The backbone and small side-chains of residues Ser209–Ser211 are stabilized *via* interactions with the area of the S2 sub-site in lobe IIb. The epsilon amino group of Trp116 is thereby prevented from fully entering the S2 sub-site. Although Trp116 also makes contact with the mercaptoethanol moiety of modified Cys351, this interaction is likely not sufficient to prevent full tryptophan rotation into the S2 sub-site (Figure 3). Supporting evidence for this mechanism might be obtained from structural analysis of unreduced calpain 1, but these experiments unfortunately failed to provide crystals. Nevertheless, the relevance of the proposed mechanism is further supported by sequence differences between human calpains 1 and 2. For instance, the human calpain 1 specific Ser209 of region α7 closely associates with lobe IIb, and

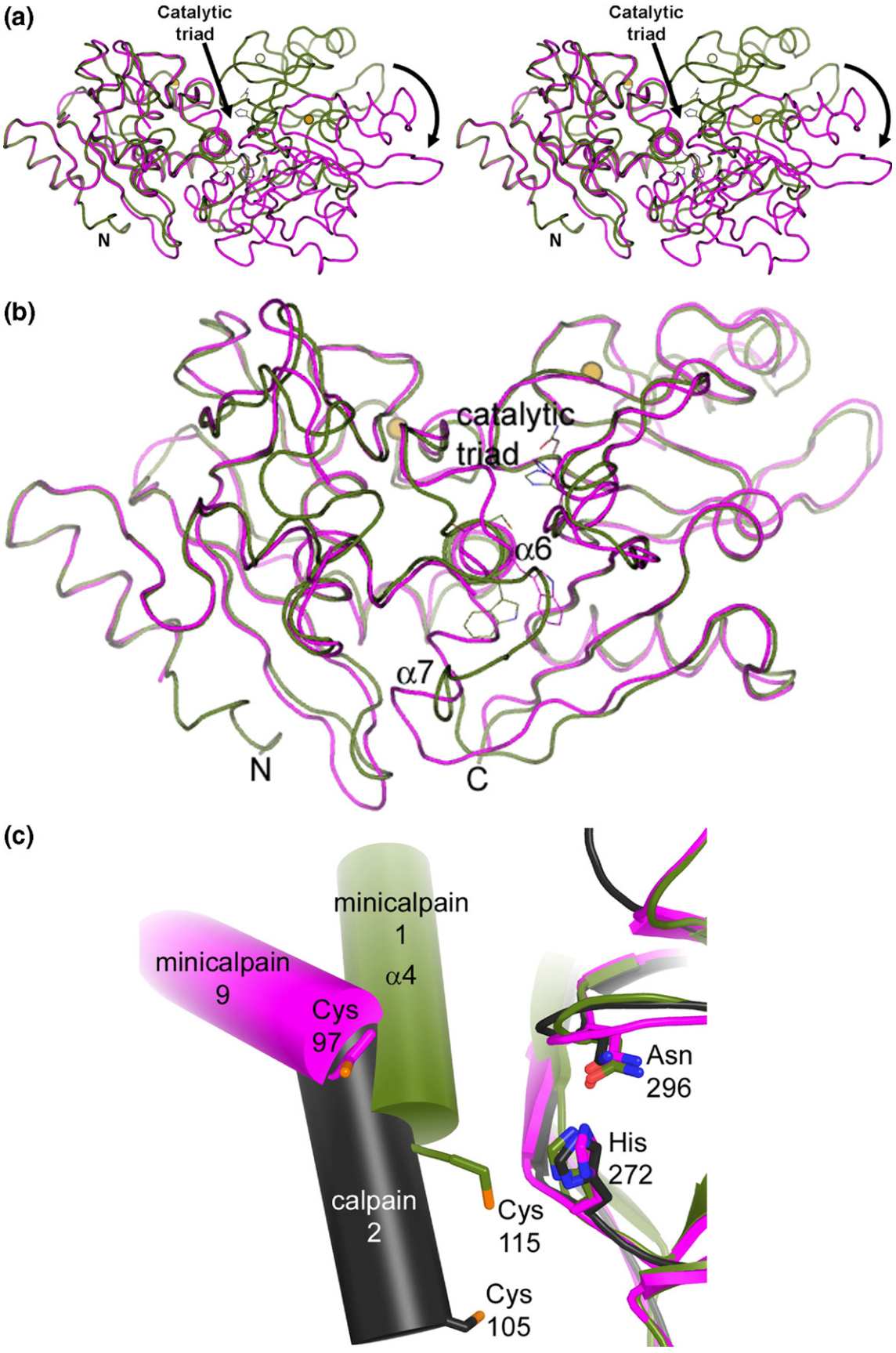

Figure 5 (*legend on opposite page*)

Table 1. Kinetic constants for hydrolysis of sLY-AMC and BODIPY-casein by minicalpains

	Human minicalpain 1	Human minicalpain 1 G213A	Human minicalpain 9	Rat minicalpain 1
sLY-AMC k_{cat} (s^{-1})	$1.39\times10^{-6}\pm4.2\times10^{-7}$	$2.16\times10^{-5}\pm7.1\times10^{-8}$	$1.67\times10^{-6}\pm8.4\times10^{-8}$	$42.7\times10^{-5}\pm4.7\times10^{-5}$
K_m (μM)	57±6	83±0.1	38±9	335±6
k_{cat}/K_m ($M^{-1}s^{-1}$)	0.024	0.259	0.035	1.275
Relative catalytic efficiency	1	11	1.5	53
BODIPY-casein (%) Relative activity(%)	100	586	105	n/a

Parameters for rat minicalpain 1 are from Moldoveanu et al.[25]

Ser211 is also involved in interactions which stabilize this arrangement of α7 (Figure 3). In contrast, a novel mechanism of auto-inhibition can be clearly seen in the minicalpain 9 structure, namely the misalignment of the catalytic lobes relative to that found in other minicalpain structures. This conformation reveals a novel aspect of calpain biochemistry.

Although intriguing, the proteolyzed catalytic core is most likely not the predominant species in cells. Regulation of activity in the full-length calpain is a complex and multi-step process. For full-length calpains 1 and 2, whose catalytic lobes are misaligned relative to each other in the inactive calcium-free state, activation requires reorientation of these lobes as well as stabilization of α7 to acquire full activity.[6,33] Minicalpains have previously only been seen in active conformations with respect to lobe orientation, best exemplified by catalytic triads that are in the proper orientation and distance to perform catalysis and by a salt bridge which connects the two lobes of the catalytic core (see e.g. Figure 1). Therefore, it has been possible when looking at these minicalpain structures to consider them almost completely competent for catalysis; the assumption made when looking at the isolated minicalpain structures solved to date (including the structure of human minicalpain 1) is that only small changes involving structural stabilization of the α7 region would be enough to recapitulate the active form of the calpain enzyme. The minicalpain 9 structure is misaligned with respect to these other minicalpain structures; however, if one independently models the two sub-domains of calpain 9 onto those of calpain 1, each lobe superimposes with an RMSD value of less than 1 Å (Figure 5(a) and (b)). More importantly, domain IIa and IIb in the minialpcain 9 structure have a relationship reminiscent of those found in the calcium-free full length calpain structures[32,33](Figure 5(c)). We therefore propose that the structure of human minicalpain 9 indicates that domains dIII and dIV of full-length calpain 9 must contribute to catalysis through proper alignment of the two catalytic lobes, rather than through stabilization of the helical α7 conformation. Our model is supported by the relative inactivity of minicalpain 9 despite the presence of an alanine, and thereby helical conformation, in α7. Its specific activity is 50-fold less than either the Gly213Ala mutant of human calpain 1 or wild-type rat calpain 1 (Table 1). It is possible that minicalpain 9 is simply not equipped to bind the sLY-AMC or BODIPY-casein substrates; indeed, our own structure analysis of the N-terminal gating loop and substrate binding sub-sites could support this idea. However, both these substrates have repeatedly been used as substrates for full-length calpains, even when later studies have shown lesser activities for isolated minicalpains compared with their full-length counterparts; and full-length calpain 9 has previously been shown in at least one study to cleave casein as a substrate.[23] CD and thermal denaturation studies of minicalpain 9 in solution indicate that the protein is well folded, contains secondary structure, and undergoes cooperative melting, all characteristics of a well-behaved protein, and consistent with the current structural determination (data not shown). The coordination of calcium ions by the isolated minicalpain core is essentially identical to the equivalent regions in both the minicalpain structures and also in the structures of the active full-length calpin structures solved previously. Taken together, this evidence indicates that the functions of calpain 9 domains dIII and dIV differ from their function in the

Figure 5. Misalignment of catalytic subdomains IIa and IIb as a mechanism of auto-inhibition in human minicalpain 9. (a) The catalytic cores of human minicalpain 1 (green) and human minicalpain 9 (magenta) are shown in ribbon representation and in stereo. In this view, sub-domains IIa are superimposed, to highlight the rotation and translation of the respective IIb sub-domains. The calcium ions for calpain 1 are shown in light yellow; the corresponding calcium ions in calpain 9 are in gold. The arrow points in the direction of rotation/translation. (b) The sub-domains IIa and IIb of calpain 9 were superimposed independently upon their counterparts in calpain 1. The RMSD value of each domain is 0.87 Å for sub-domain IIa, and 0.9 Å for sub-domain IIb. The catalytic triad is shown as sticks; calcium ions are shown in yellow. (c) The active site region of human minicalpain 9 (magenta), human minicalpain 1 (green), and the structure of full-length, calcium-free human calpain 2 (black) are shown in cartoon representation. The structures are aligned using the IIb sub-domain, as shown by the histidine and asparagine of the respective catalytic triads in stick representation. Each catalytic cysteine is labeled, but only the histidine and asparagine of calpain 9 are labeled. In this Figure, human minicalpain 1 represents the active, enzymatically competent relationship between the catalytic triad; in both the native minicalpain 9 and calcium-free full-length calpain 2 structures, sub-domains IIa and IIb are rotated and translated in such a way as to disrupt catalysis.

ubiquitous calpains, and activation by calcium will involve the formation of a catalytically competent lobe orientation by a novel mechanism. Further elucidation of the mechanism of calpain 9 activation, therefore, will almost certainly require studies of full-length protein.

The highly conserved nature of calpain cores would tend to imply a universal mechanism of catalysis and regulation. However, we present here two structures that suggest that the catalytic subunits are more complicated and undergo subtle sets of structural changes that the primary sequence cannot provide insight into. In addition, it is clear that the supporting domains in the full-length enzyme contribute more directly to full enzymatic activity than can be explained by analysis of the amino acid sequence alone. Minicalpain structures, although not directly pertinent to the discussion of the full-length enzyme, allow the analysis of a snapshot of the active site, which can provide detailed information concerning the catalytic region, the substrate binding surface, and the relationship between the catalytic lobes. These studies are important for the study and treatment of calpain-related diseases because the minicalpain region of the human calpains clearly possesses a greater degree of structural plasticity than has been previously described, making modeling of the active site inappropriate for design of specific calpain inhibitors. These studies can also allow for extrapolation to the function of the catalytic core in the context of the full-length enzyme, thereby providing potentially valuable insight into the function of the physiologically relevant form of the native enzyme.

Materials and Methods

Cloning and expression

cDNA encoding the full-length human calpain 1 (accession number NM005186) and full-length human calpain 9 (accession number NM006615) were obtained from the Mammalian Gene Collection. Ligation independent cloning was utilized to clone into the p28a-LIC vector, which contains an N-terminal $(His)_6$ tag and thrombin cleavage site. Resulting plasmids were transformed into BL21(DE3) cells (Invitrogen) for large scale protein expression. Cells were grown in a supplemented Terrific Broth media at 37 °C to an A_{600} of ~6 and induced by adding 50 μM IPTG to the cultures. Cells were induced overnight at 15 °C, then harvested and stored at −80 °C.

Purification and concentration

All chemicals were of high quality grade and purchased through Sigma unless otherwise noted. Cell pellets from 2–4 l culture were resuspended in 20 ml of lysis buffer (50 mM Tris (pH 8.0), 500 mM NaCl, 1 mM EDTA, 1 mM PMSF, 2 mM $CaCl_2$ and 0.1 ml of general protease inhibitor Sigma P2714) and then homogenized for 30–60 s per pellet. Cell lysis was accomplished by sonication (Virtis408912, Virsonic) at 4 °C; lysed cells were centrifuged in a JA25.50 rotor in an Avanti J-20 XPI centrifuge (Beckman Coulter) for 20 min at 69,673*g*. The supernatant was loaded by gravity onto 2 ml of Ni-NTA resin (Qiagen 30450). Five column volumes of lysis buffer were used to wash the column, followed by five column volumes of low imidazole buffer (lysis buffer + 10 mM imidazole (pH 8)). Samples were eluted from the Ni-NTA resin in 10 ml of elution buffer (lysis buffer + 250 mM imidazole and 10%(v/v) glycerol). For crystals obtained from protein without the $(His)_6$ tag, one unit of thrombin (Sigma T9681) per milligram of protein was then added and the protein was stored without shaking overnight at 4 °C, and all proteins were further purified using size exclusion chromatography. For gel filtration, an XK 16x65 column (18-1031-47 and 18-6488-01; GE Healthcare) packed with HiLoad Superdex 200 resin (10-1043-04; GE Healthcare) was pre-equilibrated with gel filtration buffer (lysis buffer + 5 mM β-ME, 1 mM EDTA, and 1 mM $CaCl_2$) and then samples were loaded onto the column at 1.5 ml/min, and 2 ml fractions were collected using peak fractionation protocols. Fractions were pooled and concentrated using Amicon concentrators with an appropriate molecular mass cut-off (Millipore). The protein was either used at 20 mg/ml for crystallization in the case of calpain 9, or diluted tenfold into low salt crystallization buffer (50 mM Tris (pH 8.0), 100 mM NaCl, 1 mM EDTA, and 2 mM $CaCl_2$) then re-concentrated to 20 mg/ml for crystallographic screening of calpain 1.

Crystallization, data collection, and structure solution

Calpain 1 and calpain 9 constructs were screened using in-house conditions developed by the Structural Genomics Consortium in 96 well sitting drop format using drops containing 1 μl of protein and 1 μl of reservoir. Multiple crystallization conditions were observed to produce small crystals for two constructs of calpain 1, requiring further optimization. Optimization involved, in part, elucidation of optimal pH and salt conditions for protein stability using a high-throughput differential scanning light scattering system (StarGazer) as described.[38] After optimization of the initial crystallization conditions and construct boundaries, purified calpain 1 (residues 29–360) was crystallized using the hanging drop vapor diffusion method. Diffracting crystals leading to the structure grew when the protein was mixed with the reservoir solution containing 1.5 M ammonium formate, 0.1 M Tris (pH 7.75) in a 1:1 volume ratio. Crystals typically appeared 24–36 h after incubation at 18 °C; the typical size of calpain 1 crystals was 150 μm×30 μm× 10 μm. Crystals were harvested into cryo-protection buffer (1:1 mixture of glycerol and mother liquor; final concentration of glycerol was 15%) and frozen in liquid nitrogen. In the case of calpain 9, optimization of initial crystallization conditions was also performed by the hanging drop vapor diffusion method on a construct containing residues 28–347. Diffraction quality crystals were obtained by mixing 1 μl of concentrated protein stock with 1 μl of reservoir solution containing 18–20% (w/v) PEG 3350, 0.1 M Hepes (pH 7.7), 0.2 M $CaCl_2$. Crystals typically appeared 36–72 h after incubation at 18 °C; the typical size of calpain 1 crystals was 75 μm×20 μm×10 μm. Crystals were harvested into cryo-protection buffer (1:1 mixture of glycerol and mother liquor; final concentration of glycerol was 15%) and frozen in liquid nitrogen. Diffraction data from crystals of calpain 1 were collected at beamline 19BM and

from calpain 9 at beamline 32ID, both at the Advanced Photon Source (Argonne National Laboratory), and integrated and scaled using the HKL2000 program package.[39,40] Statistics of data collection and processing are provided in Table 2.

For structure solution and refinement of calpain 1, the program PHASER[41] was used as part of the CCP4 suite[42] to find the molecular replacement solution in the resolution range between 20 Å and 2.8 Å. Initial attempts to find a molecular replacement solution with a model of the entire catalytic domain was unsuccessful, so the search model (1TLO) was subdivided into two domains. Following the successful molecular replacement search and identification of the correct space group with PHASER, a round of maximum-likelihood refinement and phase extension to 2.4 Å was carried out with REFMAC5,[42–44] and the phases were then input into ARP/wARP[42,45,46] for automatic model building and iterative refinement. The models were completed using the graphics program O[47] and further rounds of refinement using REFMAC5 resulted in an *R*-factor of 22.2% (R_{free} 26.4%) for data from 44.32 Å to 2.40 Å. The final model comprises 5142 protein atoms, 229 water molecules, four calcium ions, and two β-ME molecules for two molecules in the asymmetric unit.

For structure solution and refinement of calpain 9, the program PHASER was again used with 1MDW as a search model (subdivided into two sub-domains) in the resolution range between 20 Å and 2.5 Å. Then a round of maximum-likelihood refinement and phase extension to 2.31 Å was carried out with REFMAC5, and ARP/wARP used for automatic model building and iterative refinement. The models were completed using the graphics program O and further rounds of refinement using REFMAC5 resulted in an *R*-factor of 20.3% (R_{free} 27.2%) for data from 19.83 Å to 2.31 Å. The final model comprises 2465 protein atoms, 77 water molecules, two calcium ions, and two β-ME molecules for one protein molecule in the asymmetric unit. Both models have excellent stereochemistry as judged by PROCHECK,[48] with no residues in disallowed or unfavorable regions of Ramachandran space.

Table 2. Summary of crystallographic analysis

	Human minicalpain 9	Human minicalpain 1
A. *Data collection*		
Beamline	APS 32IDB	APS 19BM
Wavelength	1	0.97889
Resolution (D_{min}, Å)	19.83–2.31	44.32–2.40
Unique reflections	15,919	42,153
Redundancy	3.7(3.7)	8.4(3.1)
(high resolution shell)		
Completeness (%)	99.7(100)	98.9(94.6)
$\langle I/\sigma \rangle$ (high resolution shell)	19.2(3.4)	20.56(1.4)
R_{sym} (high resolution shell)	0.069(0.34)	0.089(0.569)
B. *Refinement*		
Resolution (Å)	19.83–2.31	44.32–2.40
Reflections	15,919	39,890
Number of atoms (solvent)	2552(77)	5387(229)
R_{work} (R_{free}) (%)	20.3(27.2)	22.2(26.4)
RMSD bond lengths (Å)	0.014	0.009
RMSD bond angles (deg.)	1.413	1.127
C. *Ramachandran plot*		
Most favored (%)	86.6	87.5
Additionally allowed (%)	13.4	11.9
Generously allowed (%)	0	0
Disallowed (%)	0	0

Protease activity measurements using the sLY-AMC and BODIPY-casein substrates

Activities of calpain proteases were assayed using the EnzChek kit (Invitrogen, E6638) and with a succinyl-Leu-Tyr-(7-amino-4-methylcoumarin) (sLY-AMC) peptide substrate (BACHEM, I-1335) based on previously published protocols[25,26,49,50] with modifications for use in a 384 well format. Both assays are based on the increase in fluorescence that occurs upon proteolysis of the substrate; for the BODIPY FL casein substrate, proteolysis liberates labeled casein fragments thus relieving the quenched fluorescence resulting from hyper-labeling of the casein proteins with BODIPY FL.[50] In the case of the sLY-AMC peptide the fluorescence signal increases when the AMC moiety is liberated from the peptide.[25] Briefly, 20 μM of purified protein was added to a mixture of substrate and activity buffer (100 mM Hepes (pH 7), 100 mM NaCl, 1 mM EDTA, 10 mM $CaCl_2$, and 14 mM β-ME) on ice, aliquoted into 384 well plates, and fluorescence was measured in a FluoDia T70 (Photon Technology International) at room temperature. For the sLY-AMC assay, substrate concentrations from 15 μM to 300 μM were used to ensure substrate was not limiting over the time course of the experiment; the amount of AMC released during the experiment was calculated based on a standard curve of AMC concentrations from 2 nm to 1 μM. For the BODIPY-casein assay, the total amount of label incorporated per molecule of substrate is unknown, and the activity assay was done under limiting conditions of substrate, thereby limiting analysis of the data to simple activity per time measurements. All experiments were performed in quadruplicate to reduce well-to-well variability; in addition, each protein was tested in at least three different experiments to obtain standard deviations for the parameters tested.

Protein Data Bank accession codes

The coordinates and structure factors for the structure of the protease core of human calpain 1 have been deposited into the RCSB PDB with ID 2ARY; the PDB ID for calpain 9 is 1ZIV.

Acknowledgements

This research was supported by the Structural Genomics Consortium with funds from Genome Canada through the Ontario Genomics Institute, the Canadian Institutes for Health Research, the Canada Foundation for Innovation, the Ontario Research and Development Challenge Fund, the Ontario Innovation Trust, the Wellcome Trust, GlaxoSmithKline, the Knut and Alice Wallenberg Foundation, Vinnova and the Swedish Foundation for Strategic Research. Use of the Advanced Photon Source was supported by the U. S. Department of Energy, Office of Science, Office of Basic Energy Sciences, under Contract No. DE-AC02-06CH11357.

References

1. Huang, Y. & Wang, K. K. (2001). The calpain family and human disease. *Trends Mol. Med.* **7**, 355–362.
2. Goll, D. E., Thompson, V. F., Li, H., Wei, W. & Cong, J. (2003). The calpain system. *Physiol. Rev.* **83**, 731–801.
3. Khorchid, A. & Ikura, M. (2002). How calpain is activated by calcium. *Nature Struct. Biol.* **9**, 239–241.
4. Cong, J. Y., Goll, D. E., Peterson, A. M. & Kapprell, H. P. (1989). The role of autolysis in activity of the Ca-2+-dependent proteinases (Mu-Calpain and M-Calpain). *J. Biol. Chem.* **264**, 10096–10103.
5. Cottin, P., Thompson, V. F., Sathe, S. K., Szpacenko, A. & Goll, D. E. (2001). Autolysis of mu- and m-calpain from bovine skeletal muscle. *Biol. Chem.* **382**, 767–776.
6. Reverter, D., Strobl, S., Fernandez-Catalan, C., Sorimachi, H., Suzuki, K. & Bode, W. (2001). Structural basis for possible calcium-induced activation mechanisms of calpains. *Biol. Chem.* **382**, 753–766.
7. Elce, J. S., Hegadorn, C., Simon, J. & Arthur, C. (1997). Autolysis, Ca^{2+} requirement, and heterodimer stability in m-calpain. *J. Biol. Chem.* **272**, 11268–11275.
8. Nixon, R. A. (2003). The calpains in aging and aging-related diseases. *Ageing Res. Rev.* **2**, 407–418.
9. Saito, K. I., Elce, J. S., Hamos, J. E. & Nixon, R. A. (1993). Widespread activation of calcium-activated neutral proteinase (calpain) in the brain in Alzheimer-disease – a potential molecular-basis for neuronal degeneration. *Proc. Natl Acad. Sci. USA*, 2628–2632.
10. Adamec, E., Mohan, P., Vonsattel, J. P. & Nixon, R. A. (2002). Calpain activation in neurodegenerative diseases: confocal immunofluorescence study with antibodies specifically recognizing the active form of calpain 2. *Acta Neuropathol.* **104**, 92–104.
11. Mercken, M., Grynspan, F. & Nixon, R. A. (1995). Differential sensitivity proteolysis by brain calpain of adult human-Tau, fetal human-Tau and Phf-Tau. *FEBS Letters*, **368**, 10–14.
12. Nixon, R. A. (2000). A "protease activation cascade" in the pathogenesis of Alzheimer's disease. *Alzheimers Disease: Compend. Curr. Theor.* **924**, 117–131.
13. Azuma, M., Tamada, Y., Kanaami, S., Nakajima, E., Nakamura, Y., Fukiage, C., Forsberg, N. E. *et al.* (2003). Differential influence of proteolysis by calpain 2 and Lp82 on in vitro precipitation of mouse lens crystallins. *Biochem. Biophys. Res. Commun.* **307**, 558–563.
14. Biswas, S., Harris, F., Dennison, S., Singh, J. P. & Phoenix, D. (2005). Calpains: enzymes of vision? *Medical Science Monitor*, **11**, RA301–RA310.
15. Jia, Z. C., Petrounevitch, V., Wong, A., Moldoveanu, T., Davies, P. L., Elce, J. S. & Beckmann, J. S. (2001). Mutations in calpain 3 associated with limb girdle muscular dystrophy: Analysis by molecular modeling and by mutation in m-calpain. *Biophys. J.* **80**, 2590–2596.
16. Laval, S. H. & Bushby, K. M. D. (2004). Limb-girdle muscular dystrophies – from genetics to molecular pathology. *Neuropath. Appl. Neurobiol.* **30**, 91–105.
17. Richard, I., Broux, O., Allamand, V., Fougerousse, F., Chiannilkulchai, N., Bourg, N. *et al.* (1995). Mutations in the proteolytic-enzyme calpain-3 cause limb-girdle muscular-dystrophy type-2A. *Cell*, **81**, 27–40.
18. Horikawa, Y., Oda, N., Cox, N. J., Li, X., Orho-Melander, M., Hara, M. *et al.* (2000). Genetic variation in the gene encoding calpain-10 is associated with type 2 diabetes mellitus. *Nature Genet.* **26**, 163–175.
19. Cox, N. J. (2002). Calpain 10 and genetics of type 2 diabetes. *Curr. Diab. Rep.* **2**, 186–190.
20. Paul, D. S., Harmon, A. W., Winston, C. P. & Patel, Y. M. (2003). Calpain facilitates GLUT4 vesicle translocation during insulin-stimulated glucose uptake in adipocytes. *Biochem. J.* **376**, 625–632.
21. Cox, N. J., Hayes, M. G., Roe, C. A., Tsuchiya, T. & Bell, G. I. (2004). Linkage of calpain 10 to type 2 diabetes: the biological rationale. *Diabetes*, **53**, S19–S25.
22. Yoshikawa, Y., Mukai, H., Hino, F., Asada, K. & Kato, I. (2000). Isolation of two novel genes, down-regulated in gastric cancer. *Japan J. Cancer Res.* **91**, 459–463.
23. Lee, H. J., Tomioka, S., Kinbara, K., Masumoto, H., Jeong, S. Y., Sorimachi, H. *et al.* (1999). Characterization of a human digestive tract-specific calpain, nCL-4, expressed in the baculovirus system. *Arch. Biochem. Biophy.* **362**, 22–31.
24. Markmann, A., Schafer, S., Linz, W., Lohn, M., Busch, A. E. & Wohlfart, P. (2005). Down-regulation of calpain 9 is linked to hypertensive heart and kidney disease. *Cell. Physiol. Biochem.* **15**, 109–116.
25. Moldoveanu, T., Hosfield, C. M., Lim, D., Elce, J. S., Jia, Z. & Davies, P. L. (2002). A Ca(2+) switch aligns the active site of calpain. *Cell*, **108**, 649–660.
26. Moldoveanu, T., Hosfield, C. M., Lim, D., Jia, Z. & Davies, P. L. (2003). Calpain silencing by a reversible intrinsic mechanism. *Nature Struct. Biol.* **10**, 371–378.
27. Moldoveanu, T., Campbell, R. L., Cuerrier, D. & Davies, P. L. (2004). Crystal structures of calpain-E64 and -leupeptin inhibitor complexes reveal mobile loops gating the active site. *J. Mol. Biol.* **343**, 1313–1326.
28. Li, Q. S., Hanzlik, R. P., Weaver, R. F. & Schonbrunn, E. (2006). Molecular mode of action of a covalently inhibiting peptidomimetic on the human calpain protease core. *Biochemistry*, **45**, 701–708.
29. Sorimachi, H., Ishiura, S. & Suzuki, K. (1997). Structure and physiological function of calpains. *Biochem. J.* **328**, 721–732.
30. Hosfield, C. M., Ye, Q., Arthur, J. S., Hegadorn, C., Croall, D. E., Elce, J. S. & Jia, Z. (1999). Crystallization and X-ray crystallographic analysis of m-calpain, a Ca^{2+}-dependent protease. *Acta Crystallog. sect. D, Biol.* **55**, 1484–1486.
31. Sorimachi, H. & Suzuki, K. (2001). The structure of calpain. *J. Biochem. (Tokyo)*, **129**, 653–664.
32. Reverter, D., Sorimachi, H. & Bode, W. (2001). The structure of calcium-free human m-calpain: implications for calcium activation and function. *Trends Cardiovasc. Med.* **11**, 222–229.
33. Strobl, S., Fernandez-Catalan, C., Braun, M., Huber, R., Masumoto, H., Nakagawa, K. *et al.* (2000). The crystal structure of calcium-free human m-calpain suggests an electrostatic switch mechanism for activation by calcium. *Proc. Natl Acad. Sci. USA*, **97**, 588–592.
34. Cuerrier, D., Moldoveanu, T. & Davies, P. L. (2005). Determination of peptide substrate specificity for mu-calpain by a peptide library-based approach: the importance of primed side interactions. *J. Biol. Chem.* **280**, 40632–40641.
35. Guttmann, R. P., Day, G. A., III, Wang, X. & Bottiggi, K. A. (2005). Identification of a novel calpain inhibitor using phage display. *Biochem. Biophys. Res. Commun.* **333**, 1087–1092.
36. Hosfield, C. M., Elce, J. S., Davies, P. L. & Jia, Z. (1999). Crystal structure of calpain reveals the structural basis for Ca(2+)-dependent protease activity and a novel mode of enzyme activation. *EMBO J.* **18**, 6880–6889.
37. Reverter, D., Braun, M., Fernandez-Catalan, C., Strobl, S., Sorimachi, H. & Bode, W. (2002). Flexibility analysis and structure comparison of two crystal forms of calcium-free human m-calpain. *Biolog. Chem.* **383**, 1415–1422.
38. Reinking, J., Lam, M. M. S., Pardee, K., Sampson,

H. M., Liu, S. Y., Yang, P. *et al.* (2005). The Drosophila nuclear receptor E75 contains heme and is gas responsive. *Cell*, **122**, 195–207.
39. Minor, W., Cymborowski, M. & Otwinowski, Z. (2002). Automatic system for crystallographic data collection and analysis. *Acta Physica. Polonica. A*, **101**, 613–619.
40. Otwinowski, Z. & Minor, W. (1997). Processing of X-ray diffraction data collected in oscillation mode. *Macromol. Crystallog. pt A*, **276**, 307–326.
41. Read, R. J. (2001). Pushing the boundaries of molecular replacement with maximum likelihood. *Acta Crystallog. sect. D*, **57**, 1373–1382.
42. Collaborative Computational Project, Number 4. (1994). The CCP4 suite: programs for protein crystallography. *Acta Crystallog. sect. D*, **50**, 760–763.
43. Murshudov, G. N., Vagin, A. A. & Dodson, E. J. (1997). Refinement of macromolecular structures by the maximum-likelihood method. *Acta Crystallog. sect. D*, **53**, 240–255.
44. Winn, M. D., Isupov, M. N. & Murshudov, G. N. (2001). Use of TLS parameters to model anisotropic displacements in macromolecular refinement. *Acta Crystallog. sect. D*, **57**, 122–133.
45. Lamzin, V. S. & Wilson, K. S. (1993). Automated refinement of protein models. *Acta Crystallog. sect. D*, **49**, 129–147.
46. Morris, R. J., Perrakis, A. & Lamzin, V. S. (2003). ARP/wARP and automatic interpretation of protein electron density maps. *Methods Enzymol.* **374**, 229–244.
47. Jones, T. A., Zou, J. Y., Cowan, S. W. & Kjeldgaard (1991). Improved methods for building protein models in electron density maps and the location of errors in these models. *Acta Crystallog. sect. A*, **47**, 110–119.
48. Laskowski, R. A., Macarthur, M. W., Moss, D. S. & Thornton, J. M. (1993). Procheck – a program to check the stereochemical quality of protein structures. *J. Appl. Crystallog.* **26**, 283–291.
49. Harper, J. W., Hemmi, K. & Powers, J. C. (1985). Reaction of serine proteases with substituted isocoumarins – discovery of 3,4-dichloroisocoumarin, a new general mechanism based serine protease inhibitor. *Biochemistry*, **24**, 1831–1841.
50. Thompson, V. F., Saldana, S., Cong, J. Y. & Goll, D. E. (2000). A BODIPY fluorescent microplate assay for measuring activity of calpains and other proteases. *Anal. Biochem.* **279**, 170–178.

Edited by R. Huber

(Received 12 August 2006; received in revised form 6 November 2006)
Available online 14 November 2006